Cusped Magnetic Field Mercury Ion Thruster

John R. Beattie* and Paul J. Wilbur†
Colorado State University, Fort Collins, Colo.

A residence time approach is used to explain the nonuniform beam current density profile of the SERT II thruster and to propose a magnetic field modification that should produce a highly uniform beam profile. Expressions are derived which relate the thruster performance parameters to the geometry and plasma properties of the discharge chamber. These relationships are applied to a cylindrical discharge chamber model of the SERT II thruster and suggest that, in addition to the magnetic field modication, the discharge chamber length of this thruster should be reduced. These modifications should result in a thruster that has a highly uniform beam profile, good performance, and a low double-ion population. Experimental results indicate that at about the same thrust and performance levels the beam flatness parameter of the modified thruster is 40% higher and the ratio of the double-to-single ion beam currents is about 40% lower than the values measured in the SERT II thruster.

Introduction

THE low-thrust nature of electron-bombardment ion thrusters requires long mission times to achieve the desired spacecraft velocity increment. This requirement dictates thruster designs that can operate for extended periods of time, perhaps as long as 20,000 hr.[1,2] The extension of the electron-bombardment thruster lifetime from the 100 hr or so of the earliest designs to around 10,000 hr for the more recent designs[3] has involved a somewhat systematic process of prolonging the life of individual components. During such a development program, the same thruster component may emerge periodically as the lifetime limitation. An example is the accelerator system that failed and caused the termination of the SERT II mission. The source of this failure was conjectured from the results of subsequent ground tests, and a simple solution was identified and incorporated into current thruster designs. There are, however, additional accelerator system erosion phenomena that are recognized today as posing potential life limitations: 1) erosion of the acclerator grid caused by charge-exchange ion impingement, 2) accelerator grid erosion caused by direct ion impingement, and 3) erosion of the screen grid as a result of bombardment by singly and doubly charged ions.

The objectives of this investigation were to increase the accelerator system lifetime of the SERT II thruster by 1) reducing local charge-exchange ion erosion of the accelerator grid, and 2) reducing local single- and double-ion erosion of the screen grid. One approach to the first objective is to reduce the rate of production of charge-exchange ions. Means of accomplishing this can be seen by considering the expression for the accelerator grid charge-exchange current:

$$I_{CE} = n_0 j_B \sigma_{CE} V \tag{1}$$

where

I_{CE} = accelerator grid charge-exchange current
n_0 = neutral particle density
j_B = beam current density
σ_{CE} = charge-exchange cross section
V = charge-exchange ion production volume

The charge-exchange cross section σ_{CE} is determined by the propellant and the optimum specific impulse for the mission, whereas the volume V is determined by the accelerator system design parameters (grid spacing and thickness, location of the neutralization plane, and beamlet diameter). Therefore, for a given accelerator system, the only variables remaining which are at the designer's disposal are the neutral density and beam current density. For a given propellant flow rate, the beam current density is proportional to the propellant utilization η_u, and the neutral density is proportional to the quantity $1-\eta_u$. The charge-exchange current thus can be expressed as a simple proportionality:

$$I_{CE} \propto \eta_u (1-\eta_u) \tag{2}$$

From this expression, one sees that generally the charge-exchange current can be reduced by increasing the propellant utilization. However, a practical lower limit on the charge-exchange current is imposed by the existence of the performance curve "knee."

The charge-exchange erosion damage is found experimentally to be strongly dependent on the radial coordinate, with the highest erosion rate occurring on the thruster centerline. Current density measurements in the thruster exhaust beam reveal that this profile is quite peaked at the beam centerline also. This observation, along with the dependence of the charge-exchange current on the local beam current density as illustrated by Eq. (1), explains the radial variation of the charge-exchange erosion. A quantity that describes the nonuniformity of the beam current density profile is the flatness parameter F, which is defined as the ratio of average-to-maximum beam current density. A uniform profile has a flatness parameter of 1.0, and a cosine profile, which is typical of state-of-the-art divergent field chamber designs, has a value of F equal to 0.46. This indicates that the current density at the beam center is more than twice the value that would exist with a uniform profile having the same integrated current. The dependence of the accelerator grid erosion rate on local beam current density suggests that the grid (assumed to have homogeneous composition and thickness) will wear through first in regions where the current density is a maximum. It is apparent that an improvement in accelerator grid life could be realized by distributing the charge-exchange ion erosion more evenly across the grid, and this can be accomplished by increasing the beam flatness parameter.

An approach to extending the life of the screen grid can be identified by considering the expression for the centerline value of the screen grid erosion rate:

$$W_{\ell} = \frac{I_B}{2qn\phi_s A_B F}\left[\frac{2S(E)+(J^{++}/J^{+})_{\ell}\,S(2E)}{1+(J^{++}/J^{+})_{\ell}}\right] \tag{3}$$

Presented as Paper 76-1011 at the AIAA International Electric Propulsion Conference, Key Biscayne, Fla., Nov. 14-17, 1976; submitted Dec. 1, 1976; revision received Aug. 5, 1977.

Index category: Electric and Advanced Space Propulsion.

*Graduate Student, Department of Mechanical Engineering; presently at Hughes Research Laboratories, Malibu, Calif. Member AIAA.

†Associate Professor, Department of Mechanical Engineering. Member AIAA.

where

W = screen grid erosion rate
I_B = beam current
q = electronic charge
n = number density of screen grid material
ϕ_s = screen grid open area fraction
A_B = beam area
$S(E)$ = sputtering yield of the screen grid material corresponding to the single-ion energy E
J^{++}/J^{+} = ratio of double-to-single ion current densities

Since the screen grid lifetime varies inversely with erosion rate, the preceding expression indicates that the grid life will vary linearly with the beam flatness parameter. Also, for a given accelerator system design and beam current requirement, a reduction in the ion energies and the double-to-single ion density ratio should result in a longer screen grid life.

The thrust of an electric thruster is proportional to average current density, and, using the beam flatness parameter, the proportionality can be written as

$$T \propto F j_{\max} \tag{4}$$

Since the accelerator system lifetime is determined by the maximum beam current density, Eq. (4) indicates that the thrust is directly proportional to beam flatness for a given accelerator system lifetime. Uniform beam profiles are therefore effective in 1) increasing accelerator grid lifetime at a given thrust level by reducing localized charge-exchange ion erosion, 2) increasing screen grid lifetime by reducing localized ion erosion, and 3) increasing the thrust level for a given accelerator system lifetime. Each of these improvements is of interest to the thruster designer, and together they form the basis of this investigation. Unless otherwise noted, SI (rationalized mks) units are used throughout this paper.

Discharge Chamber Theory

Residence Time Theory

A comparison of the shape of the critical magnetic field line and the beam current density profile of divergent field thruster designs reveals a striking similarity. The beam current density profile is bell-shaped, much like the upstream boundary of the primary electron region. This observation suggests that the ion density near the screen grid is a function of the distance between the critical field line and the grids, a reasonable result considering the probability of a neutral encountering an ionizing electron as it drifts through a specified region.

If one considers neutral trajectories that are parallel to the thruster axis, the length of time that a neutral atom resides in the primary electron region is given by the expression

$$\tau = L/V_0 \tag{5}$$

where

τ = neutral residence time
L = distance between the critical field line and screen grid
V_0 = neutral particle speed

In order to undergo an ionizing collison, the neutral atom must, on the average, reside in the primary electron region for a period equal to the characteristic time for ionization. The ionizing collision frequency for a neutral ground state atom interacting with primary and Maxwellian electrons is given by the expression

$$\upsilon = n_p \sigma V_p + n_m \langle \sigma V_m \rangle \tag{6}$$

where

υ = ionizing collision frequency
n_p = primary electron density
n_m = Maxwellian electron density

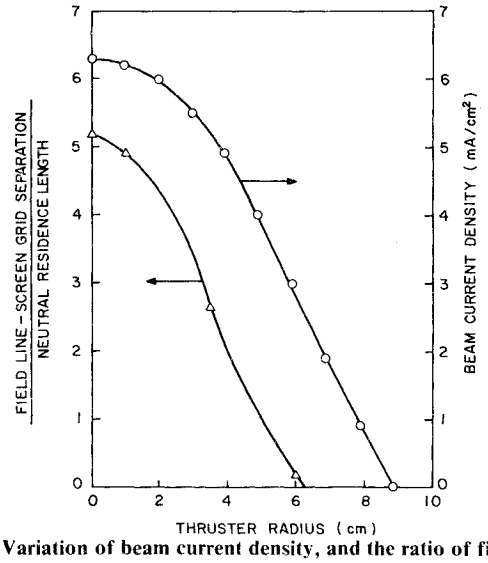

Fig. 1 Variation of beam current density, and the ratio of field line-screen grid separation to neutral residence length, with thruster radius.

V_m = Maxwellian electron speed
V_p = primary electron speed
σ = ionization cross section

The symbol $\langle Q \rangle$ denotes the average of an energy-dependent quantity Q for the Maxwellian distribution function. Equating the neutral residence time with the reciprocal of the ionization frequency results in the following expression for the minimum depth of the primary electron region:

$$L = \frac{V_0}{n_p \sigma V_p + n_m \langle \sigma V_m \rangle} \tag{7}$$

The neutral residence length L was calculated using Eq. (7) and the measured plasma properties of a SERT II divergent field thruster. An iron filings map was used to determine the distance between the critical field line and the screen grid as a function of thruster radius. The ratio of this distance to the calculated value of L at each radial position represents the probability for ionization. The results of these calculations are presented in Fig. 1, along with the measured beam current density profile of this thruster. The similarity between these profiles suggests that the neutral residence time consideration is a viable approach to shaping the beam current density profile. This implies that the beam profile can be made more uniform by increasing the neutral residence time at the periphery of the discharge chamber. Since the residence time is determined by the distance between the critical field line and screen grid, moving the field line upstream of the thruster periphery should produce the desired effect. However, this modification will increase the volume of the ion production region, and the effect of this increase on thruster performance also must be taken into account.

Performance Considerations

The SERT II thruster is a high-performance engine that was developed during an extensive test program involving over 100 discharge chamber configurations.[4] The goal of the present investigation is to improve the beam profile flatness of this thruster as a means of extending the accelerator system lifetime. At the same time, it is desirable to maintain, or perhaps improve upon, the high performance level of the SERT II thruster. For this reason, expressions relating the thruster power loss and propellant utilization to the discharge chamber geometry will be developed and used to predict thruster modifications that result in a uniform beam profile while maintaining good overall performance.

An expression for the propellant utilization efficiency can be derived by considering the single-ion production and loss

rates. It is assumed that uniform plasma properties exist within the ion production region, and that single ions are produced from the atomic ground state as a result of primary and Maxwellian electron impact. The ions are lost at the boundary of the production region at a rate given by the modified Bohm criterion.[5] Equating the production and loss rates for steady-state operation results in the following expression for the ion flux density:

$$n_i V_i = n_0 \upsilon V/A \tag{8}$$

where

n_i = ion density
n_0 = neutral density (ground energy state)
V_i = modified Bohm velocity
υ = ionization collision frequency
V/A = primary electron region volume-to-surface area ratio or characteristic length

The propellant utilization expresssion is obtained by multiplying the ion flux density by the screen grid effective open area‡ A_i and dividing by the propellant flow rate $\dot{m}$:

$$\eta_u = \frac{n_0 \upsilon A_i V/A}{\dot{m}} \tag{9}$$

The neutral loss rate and propellant flow rate are related to the propellant utilization by the expression

$$\dot{n}_0 = (1-\eta_u)\dot{m} \tag{10}$$

where $\dot{n}_0$ is the neutral loss rate and is given by the free-molecular flow expression

$$\dot{n}_0 = n_0 V_0 A_0/4 \tag{11}$$

A_0 is the effective sharp-edged orifice area of the accelerator system. Combining Eqs. (9-11) results in the desired expression for the propellant utilization:

$$\eta_u = \left(1 + \frac{V_0 A_0}{4\upsilon A_i V/A}\right)^{-1} \tag{12}$$

In deriving Eq. (12), it was assumed that single ions are produced from the atomic ground state. However, the excited states of mercury (particularly the 6^1P_1 resonance state and 6^3P_2 metastable state) contribute substantially to the total production rate.[6] To account for this, the ground state reaction rate $n_0\upsilon$ should be replaced by the total reaction rate, which includes the excited states. In the final result, the collision frequency υ can be replaced by an effective collision frequency $\bar{\upsilon}$, which is given by the following expression:

$$\bar{\upsilon} = \frac{\upsilon + \sum_i \frac{n_m^i}{n_0}\upsilon_m^i + \sum_i \frac{n_r^i}{n_0}\upsilon_r^i}{1 + \sum_i \frac{n_m^i}{n_0} + \sum_i \frac{n_r^i}{n_0}} \tag{13}$$

where the subscripts r and m refer to the resonance and metastable states, and the summation is over all excited states that contribute significantly to the production of single ions. The collision frequencies υ_m^i and υ_r^i are given by Eq. (6), with the cross section σ replaced by the cross sections σ_m^i and σ_r^i.

As a first approximation, the discharge power, or beam ion production cost, can be expressed as the product of the plasma ion production cost C_i and the ratio of primary electron region surface area to screen grid effective open area[7]:

$$P = C_i A/A_i \tag{14}$$

The plasma ion production cost represents the energy required to produce a plasma ion and consists primarily of inelastic collisional losses.

If one assumes that the plasma properties remain constant or vary in such a way that C_i and $\bar{\upsilon}$ remain constant, then Eqs. (12) and (14) can be used to demonstrate the effect of discharge chamber geometry on thruster performance. For example, Eq. (14) shows that the discharge power will remain constant if the ratio A/A_i is held fixed. This requirement and Eq. (12) indicate that the propellant utilization also remains constant if the ratio A_0/V is fixed. These results are useful scaling relationships for the thruster designer. If the primary electron region has a cylindrical shape, the performance parameters given by Eqs. (12) and (14) can be simplified to the following form by introducing the area and volume relationships for a cylinder of length l and radius r:

$$P/C_i = (2/\phi_i)(1 + l/r) \tag{15}$$

$$\eta_u = \left[1 + \frac{V_0\phi_0}{2\bar{\upsilon}\phi_i}\left(\frac{1}{l} + \frac{1}{r}\right)\right]^{-1} \tag{16}$$

ϕ_0 and ϕ_i are the effective open area fractions of the accelerator system to neutrals and ions, respectively. From these expressions, one can see the importance of a large ion open area fraction in reducing discharge losses and increasing propellant utilization. The dependence of propellant utilization on the product $V_0\phi_0$ illustrates the importance of low chamber wall temperature, high molecular weight, and low neutral open area fraction. Both the discharge power and propellant utilization depend on thruster radius in such a manner that large-diameter thrusters should perform better than small-diameter ones, a well-established experimental result. The length, on the other hand, is seen to have opposing effects on the performance parameters. This suggests that small-diameter thrusters can achieve acceptable propellant utilization efficiencies (at the cost of higher discharge losses) by increasing the chamber length. This prediction is also apparent if one considers the variation in the length-to-diameter ratios of optimum thruster designs.[8]

The results of the preceding analysis can be used for the somewhat different problem that is of interest in the present investigation. In this case, the thruster radius is fixed, and the primary electron region can be modeled by a cylinder that lies along the axis of the thruster, as illustrated in Fig. 2a. Due to the magnetic field geometry the effective radius of the cylinder is considerably smaller than the chamber radius. This confinement of the high-energy electrons to the center of the chamber results in a nonuniform beam current density profile, as illustrated in the figure. In order to achieve a more uniform beam profile, the radius of the cylindrical primary electron region can be increased by means of a magnetic field modification. The basic difference between this problem and that of increasing the thruster diameter is that in the present case the same grids are used, and thus the open area for neutral loss remains constant as the primary electron region is expanded radially outward. The effect that this change will have on the thruster performance parameters can be predicted by use of the expressions derived previously.

Equations (12) and (14) were used to calculate thruster performance as a function of cylinder length for fixed values of cylinder radius. The quantity $V_0A_0/4\bar{\upsilon}$ in Eq. (12) was evaluated using the SERT II thruster geometry and propellant utilization. Calculations were made for a cylinder radius of 4

‡The effective open area of the screen grid is sometimes greater than the geometric open area because the plasma sheath assumes a concave shape near the upstream side of the screen grid. The effect of this condition is to deflect ions into the beam which would otherwise have recombined on the screen grid.

cm, which was chosen to correspond to the SERT II thruster primary electron region, which has a volume-to-area ratio of 1.4 cm and a length at the thruster centerline of 9 cm. An equivalent cylinder having this same length and volume-to-area ratio has a radius of 4 cm. The 4-cm value also represents the radius at which the beam current density drops off rapidly, as illustrated in Fig. 1. A 6-cm cylinder radius also was considered and was chosen as representative of the radius to which the primary electron region can be expanded within a 15-cm-diam discharge chamber while maintaining adequate plasma confinement at the cylindrical chamber boundary. Different choices for the values of r would have no qualitative and little quantitative effect on the results of the calculations. The performance parameters calculated in the manner just described are presented in Fig. 3. The numbers adjacent to the symbols on these curves indicate the primary electron region length in centimeters. It is interesting to note the similarity between these curves and typical performance plots obtained in an operating thruster. The increase in primary electron region length has the same effect as increasing the power input, whereas the increase in radius has the same effect as increasing the propellant flow rate. The data of Fig. 3 indicate two important results: 1) increasing the diameter of the primary electron region produces substantial performance gains; and 2) an optimum chamber length exists for each diameter which represents a compromise between low discharge losses and high propellant utilization.

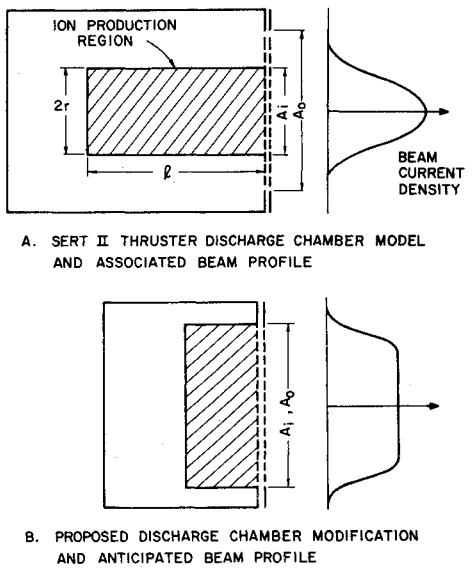

Fig. 2 Discharge chamber models and their associated beam current density profiles.

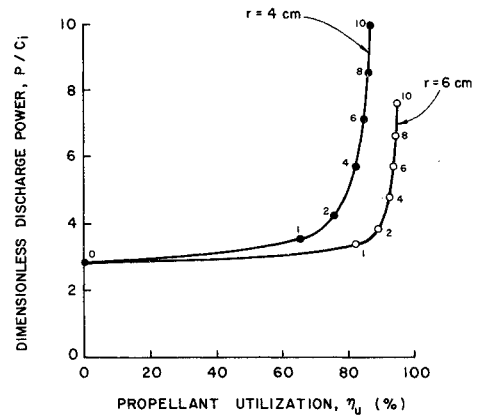

Fig. 3 Calculated discharge chamber performance resulting from chamber length variations. Numbers adjacent to the symbols indicate the primary electron region length in centimeters.

The neutral residence time and performance considerations suggest the modifications to the SERT II discharge chamber geometry illustrated in Fig. 2b. The changes consist of 1) a magnetic field modification that increases the radius of the primary electron region, and 2) a reduction in the primary electron region length. The anticipated results of these modifications are an improvement in both the uniformity of the ion beam current density profile and the thruster performance. The improvements predicted by the simple model are, of course, based on the assumption of constant plasma properties.

Double Ionization

The presence of doubly charged ions in the discharge chamber is undesirable for several reasons. Perhaps the most important of these is sputtering damage to the interior of the discharge chamber, particularly the baffle and screen grid. Therefore, the effect of the proposed discharge chamber modification on the double-ion concentration should be assessed. Theoretical studies of the double ionization processes occurring in mercury electron-bombardment thrusters[6] have shown that the majority of the double-ion production is due to electron bombardment of singly charged ions. This permits an approximate relationship for the double-to-single ion density ratio to be derived based on the assumption that double ions are produced solely from single ions. Equating the double-ion production and loss rates results in the following expression for the double-to-single ion density ratio:

$$\frac{n_{++}}{n_{+}} = \frac{\upsilon_{+}^{+\,+}\, V/A}{\sqrt{2}V_i} \tag{17}$$

The collision frequency $\upsilon_{+}^{+\,+}$ is given by Eq. (6), with the cross section σ replaced by the cross section for the production of double ions from single ions, $\sigma_{+}^{+\,+}$. Comparing Eqs. (12) and (17) reveals the dilemma confronting the ion chamber designer. In order to achieve high propellant utilization efficiencies, the discharge chamber characteristic length V/A should be large, but according to Eq. (17) this will result in a large double-ion concentration.

Fortunately, the modification proposed in Fig. 2b results in a predicted increase in the propellant utilization and a decrease in both the discharge power loss and double-to-single ion density ratio for the proper choices of the cylinder radius and length. This occurs because the open area to neutral propellant loss A_0 remains constant (the physical open area of the grids remains fixed), whereas the effective open area for ion extraction A_i increases (ion production region expanded radially). In other words, the characteristic length V/A can be reduced, causing a reduction in the double-to-single ion density ratio. At the same time, the quantity $A_i V/A$ can be increased, producing an increase in the propellant utilization; A/A_i can be reduced, producing a decrease in the discharge power loss. As an example, one might assume an initial primary electron region length and radius of 9 and 4 cm. If the primary electron region length was reduced to 4 cm and the radius increased to 6 cm, one would expect a 7% increase in propellant utilization and reductions in discharge power and double-to-single ion density ratio of 48% and 14%, respectively.

Apparatus

The discharge chamber used in this investigation is illustrated in Fig. 4, together with the SERT II thruster discharge chamber. The major difference between the two configurations is the additional soft-iron pole piece located between the cathode and anode pole pieces. This modification produced the cusped magnetic field (CMF) geometry illustrated in the figure and resulted in an increase in the neutral residence length throughout most of the chamber. The SERT II thruster permanent magnets were replaced with

electromagnets, and current to the magnet windings was provided by separate power supplies, enabling independent control of the fields produced in the regions between the pole pieces. The original soft-iron upstream end plate was replaced with an aluminum plate, and the upstream electromagnets were designed to provide a permeable path between the cathode and center pole pieces. These features insured that the minimum path length through the plasma in the upstream end of the chamber was between the pole pieces and resulted in a predominantly radial magenetic field in this region.

The cusped magnetic field geometry is produced by maintaining the cathode and anode pole pieces at the same magnetic polarity. Reversing the current direction through either set of electromagnets changes the polarity of this set and results in a divergent magnetic field geometry. This unique feature allows radical changes in the magnetic field geometry to be made during thruster operation by simply reversing a switch. The purpose of the divergent magnetic field geometry was not to duplicate the SERT II magnetic field but to allow the effects of two radically different magnetic field geometries to be evaluated with the same discharge chamber and identical operating conditions. An iron filings map illustrating the field geometries obtained with this arrangement is presented in Fig. 5.

The length of the cylindrical anode located in the downstream end of the chamber was reduced to permit the installation of the center magnet pole piece, and a disk-shaped anode was installed in the upstream end of the chamber. This anode was constructed of stainless-steel screen to facilitate uniform distribution of the neutral propellant flow to the discharge chamber. The axial position of the upstream anode can be varied during thruster operation, and this capability permits some operator control of the plasma properties and thruster performance by altering the plasma confinement at the upstream boundary of the primary electron region.

The separation distance L between the center and anode pole pieces determines the length-to-diameter ratio of the primary electron region, and this parameter is varied easily by replacing the downstream section of the chamber. The ability to vary the primary electron region length, magnetic field geometry, and anode position makes the discharge chamber

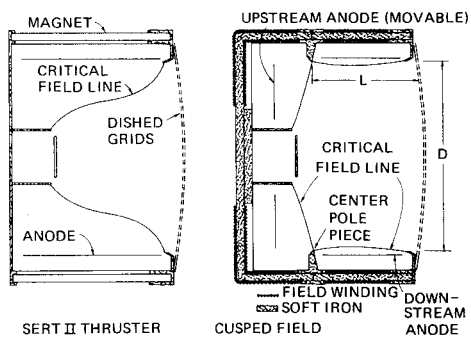

Fig. 4 Comparision of the SERT II and cusped field thruster geometries.

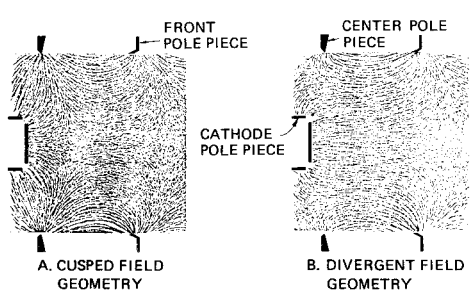

Fig. 5 Iron filings maps of the cusped and divergent magnetic field geometries ($L/D = 0.53$).

designed for this investigation a unique and flexible research tool. Some additional features include the following: 1) a variable magnetic baffle that is useful in regulating the conductivity of the plasma in the annular region between the cathode pole piece and baffle, 2) individual vaporizers that permit independent control of the main and hollow cathode flow rates, and 3) large-orifice-diameter (0.5 mm) main and neutralizer cathodes that facilitate thruster operation at high beam current conditions.

The accelerator system is a high-perveance dished type that provides good thermal stability and high beam current capacity at the specific impulse level desired for North-South stationkeeping of geosynchronous satellites. The screen electrode has a 67% open area fraction to minimize ion recombination losses, and the accelerator electrode has a 54% open area fraction to reduce neutral propellant loss. The accelerator grid is compensated to reduce the beam divergence and resultant thrust loss caused by the spherical shape of the accelerator system.

Mass flow rates are determined by timing the drop of the liquid mercury column in a precision bore glass tube, and these measurements are considered accurate to within ±3%. Plasma diagnostic information is obtained by the use of a moveable Langmuir probe.[9] The collector is 0.074-cm-diam tantalum wire, which extends 0.127 cm beyond an aluminum oxide insulator. A sliding protective sleeve is used to shield the probe and insulator when not in use, and this arrangement was found to extend the useful lifetime of the probe by preventing the accumulation of conducting sputtered material. A Faraday cup probe[9] is used to measure the ion beam current density profiles at a distance of 6 mm downstream of the accelerator grid. The double- and single-ion components of the current density profile are obtained by use of a collimating $\mathbf{E} \times \mathbf{B}$ momentum analyzer.[10]

Procedure

Thruster operating conditions were selected on the basis of using a 15-cm-diam mercury thruster to satisfy the North-South stationkeeping requirements of a 700-kg geosynchronous satellite.[11] The specific impulse and thrust requirements of this mission dictate a 600-mA beam current, with screen and accelerator grid potentials of +1000 and −500 V, respectively.[12] Typical thruster operation at the performance curve knee results in a propellant utilization efficiency of about 80-85%. This range of utilization and the desired 600-mA beam current results in a nominal propellant flow rate of 730 mA, which was the standard flow used in this investigation. A 37-V anode potential was chosen as the nominal value and represents a compromise between ionization efficiency and thruster lifetime considerations.

Three discharge chamber lengths were evaluated during this investigation and correspond to 100, 75, and 63% of the SERT II thruster length. Data were obtained for both the cusped and divergent magnetic field geometries with the upstream anode located in two different axial positions. The thruster was operated in a 1.2-m-diam 4.6-m-long vacuum facility, and during thruster operation the tank pressure was in the 10^{-6} Torr range.

Results and Discussion

Beam Profile

The cusped magnetic field geometry generally resulted in a more uniform beam profile for all discharge chamber lengths investigated, and this is in agreement with the neutral residence theory presented earlier. In general, a substantial improvement in the beam profile uniformity was realized as a result of discharge chamber length reduction. This resulted from an increased radial uniformity of the ion density profile near the screen grid because of the reduction in magnetic field fringing in the region between the center and anode pole pieces. This reduction in fringing produced a relatively field-

free region over a large fraction of the discharge chamber volume which resulted in more uniform ion density and beam current density profiles. These results suggest that the optimum discharge chamber configuration would have zero magnetic field throughout the bulk of the discharge chamber volume, with a magnetic field located near the chamber boundary to provide adequate plasma confinement. This type of discharge chamber usually is referred to as the MESC or multipole geometry and was first introduced by Ramsey[13] and Moore.[14] A modification of the earlier design has been investigated by Kaufman[15] using argon and xenon propellants, and the high ion beam flatness parameters measured by Kaufman tend to support this hypothesis. More recent investigations of a 15-cm multipole thruster operated on mercury propellant have been conducted by Wilbur.[16] However, these results indicate that the beam flatness parameter of this thruster is intermediate to the values obtained for the SERT II and cusped magnetic field geometries.

Nondimensional ion beam current density profiles are presented in Fig. 6 for the SERT II and cusped magnetic field thrusters. The integrated beam current is the same for each profile, and, when normalized in this manner, the reciprocal of the peak normalized current density is numerically equal to the beam flatness parameter. The ideal current density profile is shown in Fig. 6 for comparison. The normalized profiles indicate that a dramatic improvement over the SERT II thruster beam profile uniformity was accomplished with the cusped magnetic field discharge chamber design. The beam flatness parameter of the cusped field geometry is about 30% greater than the SERT II thruster value for the same discharge chamber length. The flatness parameter of the shorter chamber (near-optimum performance) geometries is about 40% higher than the SERT II thruster value.

Discharge Chamber Performance

The effect of reducing the discharge chamber length was to reduce the baseline discharge losses of both the cusped and divergent magnetic field thrusters by some 100 eV/ion. The baseline losses for the cusped magnetic field geometry were reduced slightly as a result of reducing the chamber length-to-diameter ratio from 0.30 to 0.23. However, the performance at the "knee" of the curve was improved slightly for the case of $L/D=0.30$. The improvement in thruster performance which accompanied the discharge chamber length reductions, as well as the existence of an optimum chamber length, is in agreement with the predictions of the discharge chamber model presented earlier. These predictions were based on the assumptions of a cylindrical ion production region and constant and uniform plasma properties and generally proved to be valid in spite of the fact that the ion production region is not cylindrical and the plasma properties varied. As a result of the plasma property variations, the plasma ion production cost C_i is an unknown variable, and therefore the discharge power losses cannot be compared with the theoretical predictions presented earlier. However, the propellant utilization as well as the double-to-single ion density ratio can be calculated by use of the expressions developed earlier and then compared with the measured values of these quantities. The calculations were made using Eqs. (12) and (17), which were derived assuming that uniform plasma properties exist within the ion production region. The fact that the plasma properties in actual thrusters have a spatial variation was taken into account by introducing an equivalent uniform property region that has the same volume as the nonuniform property region. Average plasma properties were defined for the equivalent region such that the average values yield the same ion production rate as obtained by integrating the ion production rate per unit volume over the nonuniform property region. The area of the uniform property region was reduced such that the ion loss rates calculated using the uniform plasma property values were the same as the loss rates calculated by integrating the measured ion flux rate over the boundary of the ion production region. A detailed description of the prodcedure used to calculate the volume-averaged plasma properties and the plasma nonuniformity factors used to reduce the area of the ion production region is given by Peters and Wilbur.[17] The results of the propellant utilization calculations are presented in Fig. 7, which shows good agreement between the calculated and measured values.

A performance comparison between the SERT II and the cusped magnetic field thrusters is presented in Fig. 8. (The propellant utilization data have not been corrected for the presence of multiply charged ions.) The cusped field data

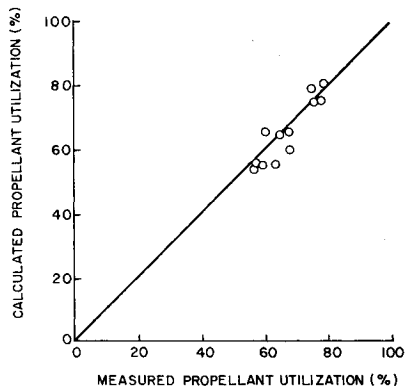

Fig. 7 Comparison of calculated and measured propellant utilization.

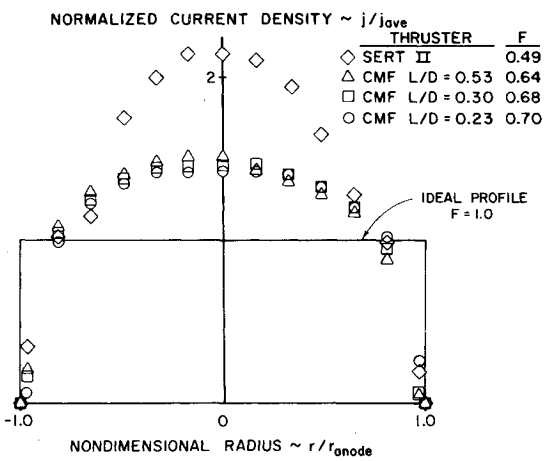

Fig. 6 Comparison of the SERT II and cusped magnetic field thruster beam current density profiles (730-mA propellant flow rate, 4-A anode current, 37-V anode potential).

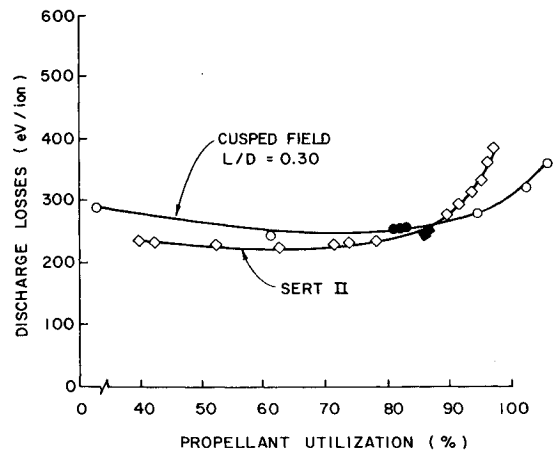

Fig. 8 Comparison of the SERT II and cusped field thruster performance (730-mA propellant flow rate).

correspond to a discharge chamber length-to-diameter ratio of 0.30 and indicate a slightly higher baseline discharge loss than the SERT II thruster. The performance at the "knee" of the curves is nearly identical for both thrusters.

Double Ionization

The ratio of the double-to-single ion beam current components is presented as a function of discharge chamber length-to-diameter ratio in Fig. 9. These results are presented for the cusped magnetic field configuration, although similar results were obtained with the divergent magnetic field geometry. The intermediate chamber length resulted in the lowest double-to-single ion current ratio, and both the intermediate and long chambers are close to optimum from the standpoint of minimum double-to-single ion current ratio. The upstream anode position resulted in optimum thruster performance, and Fig. 9 indicates that the minimum double-to-single ion current ratio obtained with this configuration is about 5%. This represents a significant reduction in the 8% value reported for the SERT II thruster.[6] In addition, the double-ion beam flatness parameter of the cusped magnetic field design was 0.4, a value that is 40% higher than that measured for the SERT II thruster.

The downstream position of the anode is generally seen to produce a slight reduction in the double-to-single ion current ratio, but it also resulted in a significant reduction in the beam current. Plasma property measurements indicated that the downstream movement of the anode caused a substantial drop in the Maxwellian electron temperature, and this lowered the single- and double-ion production rates. A model[18] was developed which relates the electron temperature to the proximity of the anode to the magnetic field lines in the upstream end of the discharge chamber. The model assumes that the anode depletes the high-energy (large cyclotron radius) electrons in the tail of the distribution function, thus lowering the temperature of the electrons. The results of the model have been found to agree quite well with experimental results for predicting both the magnitude of the temperature drop and the anode position at which the drop would occur.

Double-to-single ion density ratios were calculated using Eq. (17) and the plasma properties measured within the discharge chamber. The calculated and measured values of the double-to-single ion density ratio gave reasonable agreement; the error was of the same order reported by other investigators.[16]

Ion Production Region

In divergent field thrusters, the region of the chamber where the bulk of the ion production occurs has been defined by considering an iron filings map of the magnetic field configuration. Using this procedure, the upstream boundary of the ion production region can be approximated by the "critical" magnetic field line, which is defined as the innermost field line that intercepts the cylindrical anode. In the cusped field thruster discharge chamber, the definition of the critical field line is complicated by the presence of the additional magnet pole piece and anode. This complication prompted the development of a quantitative procedure for defining the ion production volume in an arbitrary discharge chamber design. The method developed for defining the boundary of the ion production volume consists of the following steps:

1) The plasma properties, as determined by numerical analysis[19] of Langmuir probe measurements, are used to calculate the ionization collision frequency at each probe location by use of Eq. (6). The calculated collision frequencies are normalized with respect to the maximum value, and contours of the normalized collision frequencies are determined.

2) The single- and double-ion production rates are calculated for the entire discharge chamber volume. The collision frequency contour that encloses a large fraction (e.g., 95%) of the total single- or double-ion production rate is then used as the ion production region boundary. Once the boundary has been identified, volume-averaged values for the discharge chamber plasma properties can be calculated. These volume-averaged properties are useful for comparing the various discharge chamber configurations and explaining the thruster performance characteristics.

A computer routine was developed to perform the analysis that was described above, and this routine is described in more detail by Beattie and Wilbur.[18] An example of the collision frequency contours and ion production region boundary determined by the program is presented for a divergent magnetic field geometry in Fig. 10a and for a cusped magnetic field geometry in Fig. 10b. In these figures, the solid lines represent the normalized collision frequency contours, and the broken line represents the ion production region boundary. The inner, or highest, contour is for a normalized collision frequency of 0.9, and the contour line increment is 0.1. For the examples shown, the ion production region boundary was defined as the collision frequency contour that enclosed 95% of the total single-ion production.

The procedure just described for identifying the ion production region boundary has been quite useful in the following respects:

1) This method of identifying the important region for ion production resulted in much better agreement between calculated and measured quantities, such as propellant utilization and double-to-single ion density ratio, than had been realized when the ion production region boundary was identified using iron filings maps.

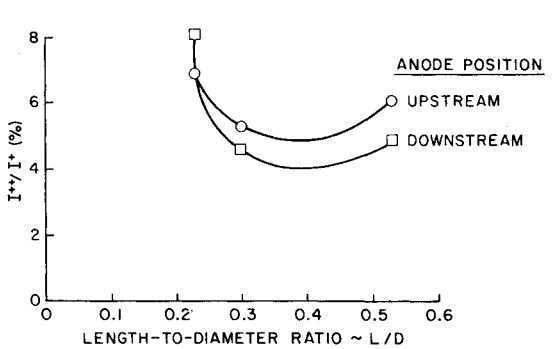

Fig. 9 Cusped magnetic field thruster double-to-single ion beam current ratio (730-mA propellant flow rate, 4-A anode current, 37-V anode potential).

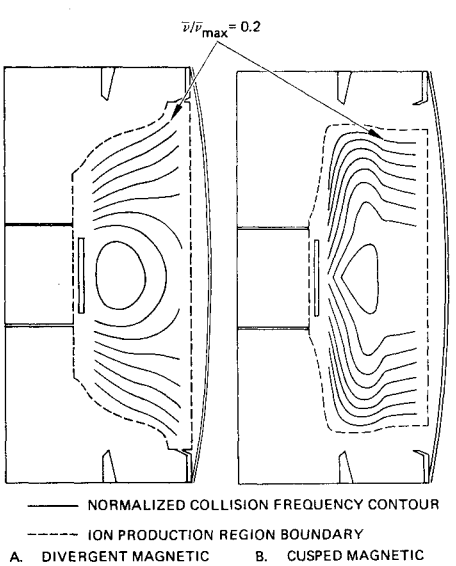

Fig. 10 Collision frequency contours and ion production region boundary ($L/D = 0.30$). Collision frequency contour increment = 0.1.

2) The collision frequency contours identify fundamental differences between the cusped and divergent magnetic field geometries. For example, the contour lines for the divergent magnetic field geometry are seen to diverge, much like the magnetic field lines. The contour lines for the cusped magnetic field geometry, on the other hand, clearly indicate a phenomenon that is not immediately obvious from considering magnetic field lines. The contour lines are drawn out toward the center magnet pole piece, indicating a high-energy density region extending radially outward from the center of the discharge chamber.

3) The ion production region boundaries clearly indicate the increase in the depth of the ion production region near the chamber boundary which was realized with the cusped magnetic field geometry.

The shape of the contour lines in the cusped magnetic field configuration results in a T-shaped ion production region. This is due to the existence of a "magnetic bottle" in the region between the cathode and center magnet pole pieces which can be visualized by considering the iron filings map of Fig. 5a. Electrons injected through the baffle aperture tend to follow field lines that terminate on the center magnet pole piece. However, as the electrons approach the pole, many are reflected by the strong magnetic field that exists there. As the reflected electrons approach the cathode pole piece, many are reflected by the strong magnetic field in this region. This trapping effect is particularly evident in Fig. 11, which shows the contours for the cusped field discharge chamber having a length equal to the SERT II thruster length.

The improvement in the beam profile uniformity which resulted from discharge chamber length reductions was discussed earlier in this section. The reason for the flatter profile was identified as an improvement in the uniformity of the plasma density profile near the screen grid, and this was attributed to a reduction in the magnetic field penetration into the discharge chamber. The collision frequency contours of Figs. 10b and 11 illustrate this effect quite vividly. The contours in the downstream end of the cusped field discharge chamber have about the same shape as the magnetic field lines in this region, and a comparison of Figs. 10b and 11 illustrates the radial expansion of the ion production region which accompanied the reduction in magnetic field fringing.

Conclusions

The most significant results of this investigation are as follows:

1) The cusped magnetic field discharge chamber design resulted in a 40% increase in the flatness parameters of both the ion beam current density profile and the double-ion beam profile of the SERT II thruster. Based on the reductions in the maximum single- and double-ion current density, the improvement in beam profile uniformity should result in about a 40% increase in the accelerator system lifetime of this thruster. The anticipated lifetime improvement is due to a reduction in the charge-exchange ion erosion of the accelerator grid and reduced sputtering of the screen grid caused by the impingement of singly and doubly charged ions.

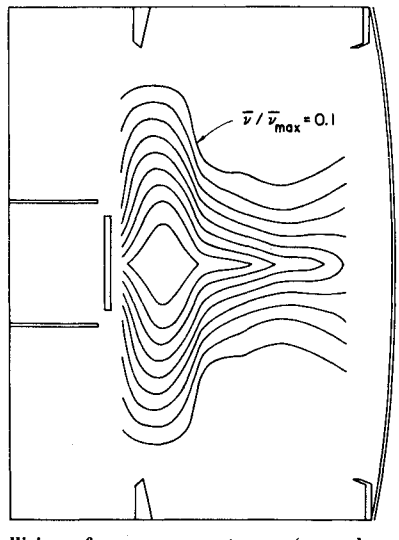

Fig. 11 Collision frequency contours (cusped magnetic field geometry, $L/D = 0.53$). Collision frequency contour increment = 0.1.

2) The performance degradation that accompanied the improvement in beam profile uniformity is relatively small: a 7% increase in the discharge power loss and a 4% reduction in the propellant utilization of the SERT II thruster.

3) Analysis of discharge chamber performance and double ionization phenomena indicated that, along with the cusped magnetic field modification to the SERT II thruster, the discharge chamber length should be reduced. Chamber length reductions were found to result in a discharge power loss reduction of 100 eV/ion, and an optimum chamber length was found. Both of these experimental results are in agreement with the predictions based on the analysis.

4) A quantitative procedure was developed and used for defining the ion production region boundary and was successful in verifying the critical field line concept of divergent field thrusters. Better agreement between theoretical calculations and experimental measurements of propellant utilization and double-to-single ion density ratio was realized using the boundary defined in this manner, as opposed to a definition based on iron filings maps.

5) The collision frequency contours indicate a fundamental difference between the cusped and divergent magnetic field geometries. The cusped magnetic field configuration tends to trap energetic electrons in a magnetic bottle region in the upstream end of the discharge chamber. This phenomenon gives rise to a T-shaped ion production region, in contrast to the bell shape of the divergent magnetic field configuration.

6) The axial position of the upstream anode was found to have a considerable effect on the thruster performance and double-to-single ion density ratio. Plasma property measurements indicated that the performance degradation and reduction in double-to-single ion density ratio associated with a downstream movement of the anode was due primarily to a substantial reduction in the Maxwellian electron temperature.

Acknowledgment

This work was performed under Grant NGR-06-002-112 sponsored by NASA.

References

[1] Hudson, W.R. and Banks, B.A., "An 8-cm Electron Bombardment Thruster for Auxiliary Propulsion," AIAA Paper 73-1131, Lake Tahoe, Nev., Oct. 1973.

[2] Hyman, J. and Poeschel, R.L., "Satellite Control Mercury Ion Thruster," AIAA Paper 73-1132, Lake Tahoe, Nev., Ot. 1973.

[3] Nakanishi, S. and Finke, R.C., "A 9700-Hour Durability Test of a 5-cm-diam Ion Thruster," AIAA Paper 73-1111, Lake Tahoe, Nev., Oct. 1973.

[4] Bechtel, R.T., "Discharge Chamber Optimization of the SERT II Thruster," *Journal of Spacecraft and Rockets,* Vol. 5, July 1968, pp. 795-800.

[5] Masek, T.D., "Plasma Properties and Performance of Mercury Ion Thrusters," AIAA Paper 69-256, Williamsburg, Va., March 1969.

[6] Wilbur, P.J., "15 cm Mercury Ion Thruster Research—1975," Colorado State Univ., Fort Collins, Colo., CR-134905, Dec. 1975.

[7] Masek, T.D., "Plasma Properties and Performance of Mercury Ion Thrusters," *AIAA Journal,* Vol. 9, Feb. 1971, pp. 205-212.

[8] Kaufman, H.R. and Cohen, A.J., "Maximum Propellant Utilization In An Electron-Bombardment Thruster," *Proceedings of the Symposium on Ion Sources and Formation of Ion Beams,* Brookhaven National Lab., Upton, N.Y., Oct. 1971, pp.61-68.

[9] Wilbur, P.J., "An Experimental Investigation of a Hollow Cathode Discharge," Colorado State Univ., Fort Collins, Colo., CR-121038, Dec. 1972.

[10] Vahrenkamp, R.P., "Measurement of Double Charged Ions in the Beam of a 30-cm Mercury Bombardment Thruster," AIAA Paper 73-1057, Lake Tahoe, Nev., Oct. 1973.

[11] Free, B.A., "Economic Tradeoff for Electric Propulsion Missions on Communications Satellites," AIAA Paper 71-683, Salt Lake City, Utah, June 1971.

[12] Wilbur, P.J., monthly letter to W.R. Kerslake, Contract Monitor, NASA Grant NGR-06-002-112, Feb. 5, 1973.

[13] Ramsey, W.D., "12-cm Magneto-Electrostatic Containment Mercury Ion Thruster Development," *Journal of Spacecraft and Rockets,* Vol. 9, May 1972, pp. 318-321.

[14] Moore, R.D., "Magneto-Electrostatically Contained Plasma Ion Thruster," AIAA Paper 69-260, Williamsburg, Va., March 1969.

[15] Kaufman, H.R., "Experimental Investigations of Argon and Xenon Ion Sources," Colorado State Univ., Fort Collins, Colo., CR-134845, June 1975.

[16] Wilbur, P.J., "15 cm Mercury Ion Thruster Research-1976," Colorado State Univ., Fort Collins, Colo., CR-135116, Dec. 1976.

[17] Peters, R.R. and Wilbur, P.J., "Double Ion Production in Mercury Thrusters," Colorado State Univ., Fort Collins, Colo., CR-135019, April 1976.

[18] Beattie, J.R. and Wilbur, P.J., "Cusped Magnetic Field Mercury Ion Thruster," Colorado State Univ., Fort Collins, Colo., CR-135047, July 1976.

[19] Beattie, J.R., "Numerical Procedure for Analyzing Langmuir Probe Data," *AIAA Journal,* Vol. 13, July 1975, pp. 950-952.